

Stochastic mixed-mode oscillations in a three-species predator-prey model

Susmita Sadhu^{1,2} and Christian Kuehn^{1,2}

¹⁾*Department of Mathematics, Georgia College & State University, Milledgeville, GA 31061, USA^{a)}*

²⁾*Department of Mathematics, Technical University of Munich, Germany^{b)}*

The effect of demographic stochasticity, in the form of Gaussian white noise, in a predator-prey model with one fast and two slow variables is studied. We derive the stochastic differential equations (SDEs) from a discrete model. For suitable parameter values, the deterministic drift part of the model admits a folded node singularity and exhibits a singular Hopf bifurcation. We focus on the parameter regime near the Hopf bifurcation, where small amplitude oscillations exist as stable dynamics in the absence of noise. In this regime, the stochastic model admits noise-driven mixed-mode oscillations (MMOs), which capture the intermediate dynamics between two cycles of population outbreaks. We perform numerical simulations to calculate the distribution of the random number of small oscillations between successive spikes for varying noise intensities and distance to the Hopf bifurcation. We also study the effect of noise on a suitable Poincaré map. Finally, we prove that the stochastic model can be transformed into a normal form near the folded node, which can be linked to recent results on the interplay between deterministic and stochastic small amplitude oscillations. The normal form can also be used to study the parameter influence on the noise level near folded singularities.

Keywords: Mixed-mode oscillations, singular Hopf bifurcation, demographic stochasticity, population outbreaks and collapses, stochastic oscillations.

Population dynamics is subject to demographic stochasticity. Dynamical models are crucial to understand the effect of this noise. We illustrate in the context of a predator-prey model the entire multi-stage process, starting from the derivation of the model using probabilistic fundamentals, to numerical simulations and concluding with links to abstract mathematical results on normal forms. We find interesting effects related to oscillation patterns, which can be constructed from a geometric phase space decomposition. Parts of the dynamics are slow, and essentially metastable, until sudden fast tipping events occur, either induced by noise or by deterministic slow drift. The resulting MMOs can be viewed as switching in a multi-stable system.

I. INTRODUCTION

Stochasticity or variability plays an important role in understanding the dynamics of predator-prey populations. In many cases, it helps to explain observable population phenomena such as random fluctuations in population densities of small mammals and forest insects^{3,23,31}. Higher per-capita growth rate of the prey than its predators can be modeled to naturally give rise to systems of singularly-perturbed differential equations^{14,21,34,36}. Noise in such models can lead to several

interesting dynamical effects, which are not anticipated by their deterministic counterpart³⁷.

There are several ways to model variability in population ecology¹³. These include variations between individuals usually referred to as demographic stochasticity, or variations caused by temporal changes in the environment, usually called environmental variations. In this paper, we will assume that variations in between individuals, follows a certain probability distribution. In this form of modeling, all individuals in the same population are treated as identical in all aspects of phenotype, and the randomness enters as a within-individual process having the same probability distribution for every individual regardless of its phenotype. We build a stochastic model, and derive when the population sizes are large, that the dynamics is approximated by a system of SDEs. A similar approach to modeling two or more interacting populations with demographic stochasticity naturally built-in has been considered in^{1,2}.

We consider the stochastic dynamics between three interacting populations, two predators competing for their common prey, under two different timescales. The deterministic model, i.e., the drift terms in the SDEs, has been extensively studied in^{35,36,38}. Of the many interesting dynamics that the deterministic model shows are MMOs, which are concatenations of small and large amplitude oscillations^{11,15,28}. The MMO cycles are ecologically significant as they qualitatively represent natural fluctuations in the population densities of species as observed in the wild. Taking demographic stochasticity into account, we obtain the interactions in the framework of a fast-slow system of SDEs. We focus our study regarding noise effects in a parameter regime near the singular Hopf bifurcation, where noise-induced MMOs are observed. To the best of our knowledge, noise-induced MMOs in three interacting populations have not been previously explored. Our results show

^{a)}Electronic mail: susmita.sadhu@gcsu.edu

^{b)}Electronic mail: ckuehn@ma.tum.de

that the distance to the singular Hopf bifurcation and noise level are crucial parameters for formation of different oscillation patterns. Large noise levels lead to stochastic extinction events, while very low noise levels preclude frequent noise-induced large amplitude oscillations (LAOs). Furthermore, parts of canard-type orbits near unstable manifolds are kicked away by small perturbations, thus “regularizing” the Poincaré map. Therefore, we conclude that optimal finite-size noise is beneficial in those predator-prey systems, where switching between alternating ecological regimes may be desirable. Hence, our model is a more complex example of the classical paradigms of stochastic/coherent resonance^{5,18,33}, which are frequently studied in neuroscience³⁰, and also provides a new direction to explore other noise-induced mechanisms²⁷.

In this paper we make an attempt to understand the interplay between singularities in fast-slow systems and noise, which has gained considerable attention recently^{6,8}. We therefore transform our system to a suitable normal form locally; this seems to be the first three-dimensional realistic SODE model with multiplicative noise, where such a transformation near folded nodes has been carried out. Finally, we compare our model results to theoretical predictions. In summary, we have provided a paradigmatic example from applications, where we combine modeling, stochastic fast-slow systems, numerical simulations and algebra to gain insight into oscillatory patterns and multi-stability.

The paper is organized as follows. In Section II, we introduce the deterministic model and review relevant theory of fast-slow systems. Existence of folded nodes and canards are also discussed in that section. In Section III, we build our main fast-slow stochastic model, we perform numerical simulations and discuss the results. In Section IV, the stochastic model is transformed to its normal form and the implications are discussed. The derivation of the normal form is provided in Appendix V.

II. THE DETERMINISTIC MODEL

Before we can start with the full stochastic model, we have to understand the deterministic aspects of the dynamics. This part forms the skeleton of our analysis as we are interested in small stochastic perturbations of deterministic dynamics. The deterministic model in its non-dimensional form with the derivation details provided in³⁸ reads as

$$\begin{cases} \frac{dx}{dt} = x' = x \left(1 - x - \frac{y}{\beta_1 + x} - \frac{z}{\beta_2 + x} \right), \\ \frac{dy}{dt} = y' = \zeta_1 y \left(\frac{x}{\beta_1 + x} - c \right), \\ \frac{dz}{dt} = z' = \zeta_2 z \left(\frac{x}{\beta_2 + x} - d - hz \right), \end{cases} \quad (1)$$

where x is the normalized population density of the prey and y and z are the normalized population densities of the predators. We always restrict our study to the first

quadrant $x \geq 0, y \geq 0, z \geq 0$ due to the natural non-negativity assumption in population dynamics. The parameters $\zeta_1, \zeta_2, \beta_1, \beta_2, c, d$ and h represent the following:

- ζ_1, ζ_2 denote the ratios of the maximum per capita growth rates of the predators y and z respectively to the per-capita growth rate of the prey. We will assume that $0 < \zeta_1, \zeta_2 \ll 1$ and fix $\zeta_1 = \zeta_2 =: \zeta$.
- The parameters β_1 and β_2 are dimensionless semi-saturation constants measured against the prey's carrying capacity. We will assume that the predators will reach the half of their maximum predation rates before the prey population reaches its carrying capacity implying that $0 < \beta_1, \beta_2 < 1$.
- The parameters c and d denote the ratios of the growth rates of the predators to their death rates. We will make the natural assumption that $0 < c, d < 1$.
- The parameter h is associated with the intraspecific competition in the class of z . In our context, $h > 1$ will indicate the presence of a strong intraspecific competition while $0 < h < 1$ will indicate a weaker competition.

With the assumption $\zeta \ll 1$, we obtain a singularly perturbed system in one fast and two slow variables which can be written on the fast time scale as

$$\begin{cases} x' = x \left(1 - x - \frac{y}{\beta_1 + x} - \frac{z}{\beta_2 + x} \right) := xu(x, y, z), \\ y' = \zeta y \left(\frac{x}{\beta_1 + x} - c \right) := \zeta yv(x, y, z), \\ z' = \zeta z \left(\frac{x}{\beta_2 + x} - d - hz \right) := \zeta zw(x, y, z), \end{cases} \quad (2)$$

where $u(x, y, z), v(x, y, z), w(x, y, z)$ represent the non-trivial x, y and z nullclines. Hence, we may apply techniques from fast-slow systems²⁸. The *critical manifold* \mathcal{M} is the set of equilibria of the fast subsystem, i.e.

$$\mathcal{M} = \{(x, y, z) : x = 0 \text{ or } u(x, y, z) = 0\} =: \mathcal{T} \cup \mathcal{S},$$

where $\mathcal{T} = \{(0, y, z) : y, z \geq 0\}$, $\mathcal{S} = \{(x, y, z) : u(x, y, z) = 0\}$. The critical manifold consists of two normally attracting sheets \mathcal{S}^a and \mathcal{T}^a , and two repelling sheets \mathcal{S}^r and \mathcal{T}^r , separated by two curves of singularities \mathcal{F}^+ and \mathcal{F}^- ^{35,38}. The normally hyperbolic parts perturb to slow manifolds by Fenichel's Theorem^{17,28}. The curve \mathcal{F}^- of transcritical points is the intersection of \mathcal{T} with \mathcal{S} . The curve $\mathcal{F}^+ = \{(x, y, z) : u(x, y, z) = 0, u_x(x, y, z) = 0\}$ is a curve of fold points. On rescaling $s := \zeta t$, (2) transforms to an equivalent system written on the slow time scale s . On letting $\zeta \rightarrow 0$ on this scale, one obtains the slow subsystem (or reduced subsystem). The corresponding dynamics is referred to as the slow flow which is restricted to the plane $\{x = 0\}$ or to the surface $\mathcal{S} := \{(x, y, z) : u(x, y, z) = 0\}$. Since $u_y \neq 0$ on \mathcal{S} , the implicit function theorem implies that \mathcal{S} can be

locally written as a graph of $y = \phi(x, z)$. Differentiating $u(x, y, z) = 0$ implicitly with respect to slow time yields

$$u_x \dot{x} + u_y \dot{y} + u_z \dot{z} = 0, \quad \frac{d}{ds} = \cdot.$$

Consequently, the slow flow restricted to \mathcal{S} reads as

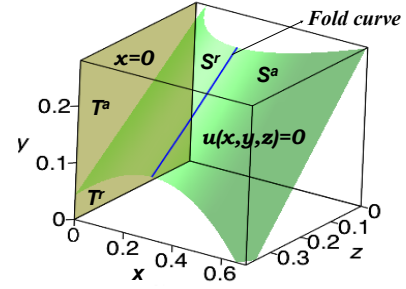
$$\begin{pmatrix} -u_x \dot{x} \\ \dot{z} \end{pmatrix} = \begin{pmatrix} u_y y v + u_z z w \\ z w \end{pmatrix} \Big|_{y=\phi(x,z)}. \quad (3)$$

Multiplying the vector field by a factor $-u_x$, and then using a suitable time re-scaling, transforms (3) to the desingularized system

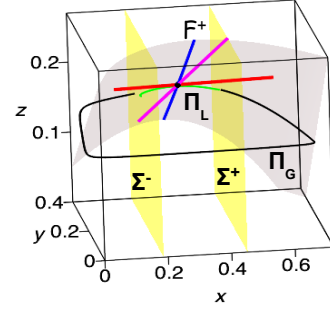
$$\begin{pmatrix} \dot{x} \\ \dot{z} \end{pmatrix} = \begin{pmatrix} u_y y v + u_z z w \\ -u_x z w \end{pmatrix} \Big|_{y=\phi(x,z)}. \quad (4)$$

The set of all points on \mathcal{F}^+ for which $u_y y v + u_z z w \neq 0$ corresponds to jump points and are said to satisfy the normal switching condition^{4,28,39}. At these points, solutions jump from \mathcal{S}^a to \mathcal{T}^a . Similarly, one can treat jump points at the curves of transcritical singularities in $\mathcal{T}^{24,29}$. This gives rise to relaxation-oscillation dynamics as shown in Fig. 1(b). Points on \mathcal{F}^+ that violate the normal switching condition are known as folded singularities^{4,28,39}. These are equilibria of the desingularized system (4). Folded singularities can be classified into their equilibrium type, e.g., one generically obtains folded nodes, folded foci and folded saddles without parameter variation; further degeneracies occur, e.g., folded-saddle nodes^{25,41} and/or singular Hopf bifurcation^{10,20}.

Under suitable parameter values, the desingularized system (4) admits a folded node singularity (x^*, y^*, z^*) . Suppose that λ_s, λ_w are the eigenvalues of the Jacobian corresponding to (4) at (x^*, y^*, z^*) such that $\lambda_s < \lambda_w < 0$. The perturbation for $0 < \zeta \ll 1$ of trajectories tangent to the eigendirections for $\zeta = 0$ corresponding to eigenvalues λ_s, λ_w gives rise to primary canards, known as the strong canard, and the weak canard denoted by γ_s and γ_w , respectively^{4,28,39,41}. The singular funnel refers to the region on \mathcal{S}^a bounded by the strong canard and the fold curve \mathcal{F}^+ . It contains trajectories flowing through the folded node. For $0 < \zeta \ll 1$, these trajectories experience small rotations around the weak canard until they jump to the other attracting sheet of the manifold \mathcal{T}^a . A global return mechanism can re-inject trajectories to the folded-node funnel to induce MMOs. The global return mechanism can be represented by a return map $\Pi : \Sigma^+ \rightarrow \Sigma^+$, where Σ^+ is a cross-section orthogonal to the x -axis away from the fold \mathcal{F}^+ such that for small ζ , all trajectories that are projected into the slow manifold \mathcal{S}_ζ^a onto a neighborhood of the funnel intersect with Σ^+ . As shown in Fig. 1(b), the map Π can be decomposed as $\Pi = \Pi_G \circ \Pi_L$, where $\Pi_L : \Sigma^+ \rightarrow \Sigma^-$ defines the local map near the fold (shown in green) and $\Pi_G : \Sigma^- \rightarrow \Sigma^+$ the global return map (in black)^{15,26}. We will study a stochastic variant of one part of this return map in Section III.



(a) The critical manifold.



(b) Existence of a global return mechanism

FIG. 1: (a): The critical manifold $\mathcal{M} = \mathcal{S} \cap \mathcal{T}$. (b): The folded node is represented by a black dot, the strong and weak eigendirections are represented by red and magenta lines respectively. The singular funnel is the region between the blue and the red curves. ^a

^a Reprinted from³⁸, Copyright (2017) with permission from Elsevier.

Suppose we are in a parameter regime such that (2) has a folded node singularity at (x^*, y^*, z^*) . Consider the eigenvalue ratio

$$\mu := \lambda_w / \lambda_s. \quad (5)$$

Then one may conclude^{28,39,41}, for sufficiently small $\zeta > 0$, the strong singular canard γ_s perturbs to a maximal canard γ_s^ζ and if $\mu^{-1} \notin \mathbb{N}$, the singular weak canard γ_w perturbs to a maximal canard γ_w^ζ . Moreover if $k \in \mathbb{N}$ be such that

$$2k - 1 < \mu^{-1} < 2k + 1 \quad \text{and} \quad \mu^{-1} \neq 2(k + 1),$$

there exists k other additional canards referred to as secondary canards. In this case, the strong singular canard γ_s twists around the primary weak canard γ_w^ζ . The j -th secondary canard γ_j^ζ , $1 \leq j \leq k$ twists $2j + 1$ times around γ_w^ζ . The twisting occurs in an $O(\sqrt{\zeta})$ -neighborhood of the folded node (x^*, y^*, z^*) . This mechanism induces small-amplitude oscillations (SAOs). A related mechanism of SAO generation is the case, when a folded saddle-node of type II occurs in system (4), or more commonly, a singular Hopf bifurcation occurs in system (2)^{20,28,39}.

In this case, SAOs are induced by dynamics near an equilibrium point of the full system with complex conjugate eigenvalues¹⁵. To illustrate this in our context, we fix the parameter values to

$$\zeta = 0.01, \beta_1 = 0.5, \beta_2 = 0.25, c = 0.38, d = 0.17 \quad (6)$$

and view h as the main bifurcation parameter. Then as discussed in³⁵, system (2) exhibits a Hopf bifurcation at

$$h \approx 2.6413 \quad (\text{Hopf of the full system}) \quad (7)$$

and the desingularized system (4) undergoes a folded saddle-node bifurcation of type II at

$$h \approx 2.722 \quad (\text{FSN II in singular limit}). \quad (8)$$

Hence, the deterministic model shows many classical features, which have been studied in other fast-slow system models, mainly in chemical reactions and neuroscience²⁸.

III. THE STOCHASTIC MODEL

In this section, we will build and analyze a stochastic variant of (2). Our first step is to justify the structure of the noise terms from a microscopic description while modeling the birth and death processes of the species as continuous time Markov processes on a discrete state space. We will consider large population sizes so that we can apply the law of large numbers allowing us to use continuous variables and differential equations in a mean-field limit¹⁹. A similar approach has been taken in¹² for modeling the interactions between a predator and its prey, where the authors consider a hybrid model treating the predator as a continuous variable and the prey as discrete. In our work, the evolution of the three species are assumed to take discrete values. To this end, let $\omega_1 x(t)$ be an integer denoting the number of prey at time t . In other words, x units of prey corresponds to $\omega_1 x$ individuals. Similarly, let $\omega_2 y(t)$ and $\omega_3 z(t)$ be integers denoting the number of two different predator species at time t .

Suppose that $\omega_1 x$ follows an exponential distribution with parameter λ_x with expectation $1/\lambda_x$, where $\lambda_x = \omega_1/\zeta$. Then the number of events N_x in terms of births and deaths during $[s, s + ds]$ is approximately

$$N_x \approx \frac{ds}{(1/\lambda_x)} = \frac{\omega_1}{\zeta} ds.$$

Let X_i be the random variable representing a change in the prey population at the i -th event. Suppose that X_i equals 1 if a birth occurs, -1 if a death occurs and 0 if no changes occur with the following probabilities:

$$\begin{aligned} \mathbb{P}(X_i = 1) &= \frac{x}{1 + x + x^2 + \frac{xy}{\beta_1 + x} + \frac{xz}{\beta_2 + x}}, \\ \mathbb{P}(X_i = -1) &= \frac{x^2 + \frac{xy}{\beta_1 + x} + \frac{xz}{\beta_2 + x}}{1 + x + x^2 + \frac{xy}{\beta_1 + x} + \frac{xz}{\beta_2 + x}}, \\ \mathbb{P}(X_i = 0) &= \frac{1}{1 + x + x^2 + \frac{xy}{\beta_1 + x} + \frac{xz}{\beta_2 + x}}. \end{aligned}$$

Then the expectation and the variance of the random variables X_i and $\sum_{i=1}^{N_x} X_i$ read as

$$\begin{aligned} \mathbb{E}(X_i) &= \frac{x - x^2 - \frac{xy}{\beta_1 + x} - \frac{xz}{\beta_2 + x}}{1 + x + x^2 + \frac{xy}{\beta_1 + x} + \frac{xz}{\beta_2 + x}}, \\ \mathbb{E}\left(\sum_{i=1}^{N_x} X_i\right) &= \frac{\omega_1}{\zeta} \left(x - x^2 - \frac{xy}{\beta_1 + x} - \frac{xz}{\beta_2 + x}\right) ds, \\ \sigma^2(X_i) &= \mathbb{E}(X_i^2) - (\mathbb{E}(X_i))^2, \\ \sigma^2\left(\sum_{i=1}^{N_x} X_i\right) &= \frac{\omega_1}{\zeta} F_1^2(x, y, z) ds, \end{aligned}$$

where

$$F_1^2(x, y, z) = \frac{x + \left(x^2 + \frac{xy}{\beta_1 + x} + \frac{xz}{\beta_2 + x}\right)(1 + 4x)}{1 + x + x^2 + \frac{xy}{\beta_1 + x} + \frac{xz}{\beta_2 + x}}. \quad (9)$$

Assuming that ω_1 is sufficiently large, from the central limit theorem, $\sum_{i=1}^{N_x} X_i$ can be approximated by a Gaussian random variable:

$$\sum_{i=1}^{N_x} X_i \approx \frac{\omega_1}{\zeta} f_1(x, y, z) ds + \sqrt{\frac{\omega_1}{\zeta}} F_1(x, y, z) W_s^x,$$

where W_t^x is the standard one-dimensional Wiener process, $F_1(x, y, z)$ is the positive square root of (9) and

$$f_1(x, y, z) = x - x^2 - \frac{xy}{\beta_1 + x} - \frac{xz}{\beta_2 + x}. \quad (10)$$

Since the variable x represents the number of individuals of prey divided by ω_1 , the increment in x during $[s, s + ds]$ will be thus given by

$$x(s + ds) - x(s) = \frac{f_1(x, y, z)}{\zeta} dt + \frac{F_1(x, y, z)}{\sqrt{\omega_1 \zeta}} W_s^x \quad (11)$$

Similarly, assume that $\omega_2 y$ and $\omega_3 z$ follow exponential distributions with parameters λ_y and λ_z respectively, where $\lambda_y = \omega_2$ and $\lambda_z = \omega_3$. Let Y_i and Z_i be the random variables representing changes in the populations of the predators at the i -th event taking values ± 1 or 0 with probabilities given in Table I.

Random variable	Probability
$Y_i = 1$	$\frac{\frac{xy}{\beta_1 + x}}{1 + \frac{xy}{\beta_1 + x} + cy}$
$Y_i = -1$	$\frac{\frac{cy}{\beta_1 + x}}{1 + \frac{xy}{\beta_1 + x} + cy}$
$Y_i = 0$	$\frac{1}{1 + \frac{xy}{\beta_1 + x} + cy}$
$Z_i = 1$	$\frac{\frac{xz}{\beta_2 + x}}{1 + \frac{xz}{\beta_2 + x} + dz + hz^2}$
$Z_i = -1$	$\frac{\frac{dz + hz^2}{\beta_2 + x}}{1 + \frac{xz}{\beta_2 + x} + dz + hz^2}$
$Z_i = 0$	$\frac{1}{1 + \frac{xz}{\beta_2 + x} + dz + hz^2}$

TABLE I: Probabilities associated with the changes

Then similar to the derivation of increment of x , the increments of y and z in the time interval $[s, s + ds]$ are given by the equations

$$y(s + ds) - y(s) = f_2(x, y, z)ds + \frac{F_2(x, y, z)}{\sqrt{\omega_2}} W_s^y \quad (12)$$

$$z(s + ds) - z(s) = f_3(x, y, z)ds + \frac{F_3(x, y, z)}{\sqrt{\omega_3}} W_s^z \quad (13)$$

respectively, where

$$f_2(x, y, z) = \frac{xy}{\beta_1 + x} - cy, \quad (14)$$

$$f_3(x, y, z) = \frac{xz}{\beta_1 + x} - dz - hz^2, \quad (15)$$

$$F_2(x, y, z) = \sqrt{\frac{\frac{xy}{\beta_1 + x} + cy + \frac{4cxy^2}{\beta_1 + x}}{1 + \frac{xy}{\beta_1 + x} + cy}}, \quad (16)$$

$$F_3(x, y, z) = \sqrt{\frac{\frac{xz}{\beta_2 + x} + \left(1 + \frac{4xz}{\beta_2 + x}\right)(dz + hz^2)}{1 + \frac{xz}{\beta_2 + x} + dz + hz^2}}. \quad (17)$$

Denoting $\sigma_i = 1/\sqrt{\omega_i}$ for $i = 1, 2, 3$ and X_t , Y_t and Z_t as the random variables for the three interacting populations, combining equations (11)-(13), we thus obtain a system of SDEs interpreted in Itô-sense:

$$\begin{cases} dX_s = \frac{1}{\zeta} f_1(X_s, Y_s, Z_s) ds + \frac{\sigma_1}{\sqrt{\zeta}} F_1(X_s, Y_s, Z_s) dW_s^{(1)} \\ dY_s = f_2(X_s, Y_s, Z_s) ds + \sigma_2 F_2(X_s, Y_s, Z_s) dW_s^{(2)} \\ dZ_s = f_3(X_s, Y_s, Z_s) dt + \sigma_3 F_3(X_s, Y_s, Z_s) dW_s^{(3)}, \end{cases} \quad (18)$$

where f_i, F_i are given by equations (9)-(10) and (14)-(17) for $i = 1, 2, 3$.

Rescaling $s = \zeta t$ and using the scaling law of Brownian motion, the equivalent fast time scale system of SDEs reads as

$$\begin{cases} dX_t = f_1(X_t, Y_t, Z_t)dt + \sigma_1 F_1(X_t, Y_t, Z_t)dW_t^{(1)} \\ dY_t = \zeta f_2(X_t, Y_t, Z_t)dt + \sqrt{\zeta} \sigma_2 F_2(X_t, Y_t, Z_t)dW_t^{(2)} \\ dZ_t = \zeta f_3(X_t, Y_t, Z_t)dt + \sqrt{\zeta} \sigma_3 F_3(X_t, Y_t, Z_t)dW_t^{(3)}. \end{cases} \quad (19)$$

Systems (18) and (19) are referred to as stochastic fast-slow systems with X being the fast and Y, Z being the slow variables, and σ_i for $i = 1, 2, 3$ are the corresponding noise parameters.

Note that σ_i^2 is inversely proportional to the size of the population. For larger population size we can expect the deterministic part of the process to dominate on quite long time scales⁶. Consequently, on these time scales, extremely small values of σ_i (for instance, $\sigma_1 = 10^{-7}, \sigma_2 = \sigma_3 = 10^{-4}$) lead to only very small deviations from the deterministic model (2).

Larger values of σ_i (such as $\sigma_1 = 10^{-5}, \sigma_2 = \sigma_3 = 10^{-4}$) can lead to extinction of species. This is easy to see from our derivation as the noise terms vanish when the population sizes are zero.

Interestingly, for intermediate values of σ_i (for instance, $\sigma_1 = 10^{-6}, \sigma_2 = \sigma_3 = 3 \cdot 10^{-4}$), we observe

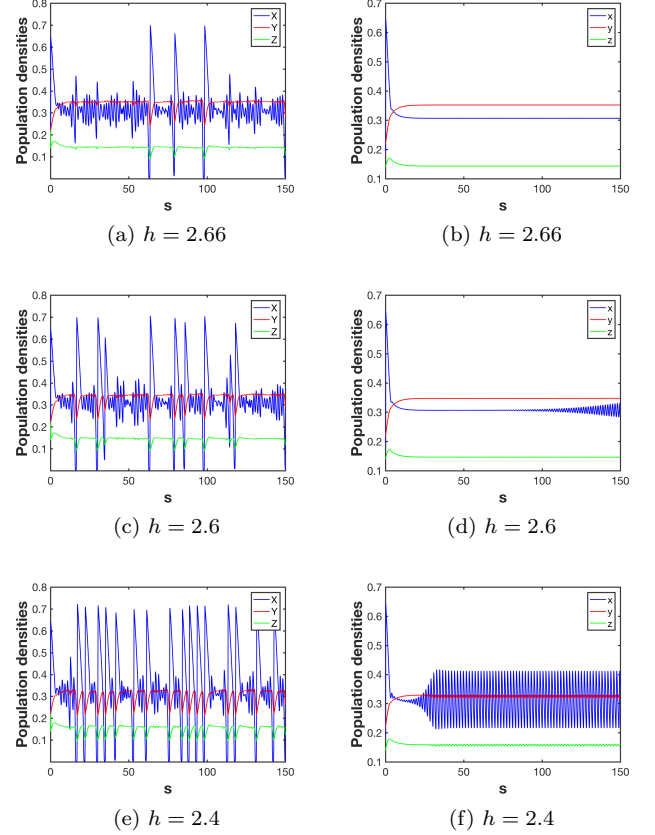


FIG. 2: Left column: Time series of different sample paths of system (18) as h is varied. Note the existence of isolated spikes and repeated spikes. Right column: Time series of the deterministic system (2) on the slow time scale for varying h . The other parameter values are given by (6) with $\sigma_1 = 10^{-6}$, $\sigma_2 = \sigma_3 = 3 \cdot 10^{-3}$.

different kinds of noise-induced MMOs as shown in the numerical simulations²² in Fig. 2. The isolated/repeated spikes in the time series in Fig. 2 represent events of random population outbreaks or collapses as documented for small mammals and insects in the wild^{3,23,31}. We also observe that the noise-driven dynamics can be significantly different depending on how close we are to the singular Hopf bifurcation; cf. (7)-(8). Indeed, if we are below it, we see rare excursions giving rise to LAOs (isolated spikes). On the other hand, in the near Hopf-regime, due to the small stable limit cycle generated at the (singular) Hopf bifurcation, which has a part near an unstable slow manifold¹⁵, the noise can induce LAOs more frequently. This means we really see noise-generated MMOs with two different characteristics.

Fig. 2 also suggests the presence of an intricate interplay between the noise-induced SAOs and the SAOs initiated by the drift terms. To investigate this effect further, we consider the number of SAOs between two spikes and denote it by N . The distribution of N for 200 different sample paths near the Hopf bifurcation are shown

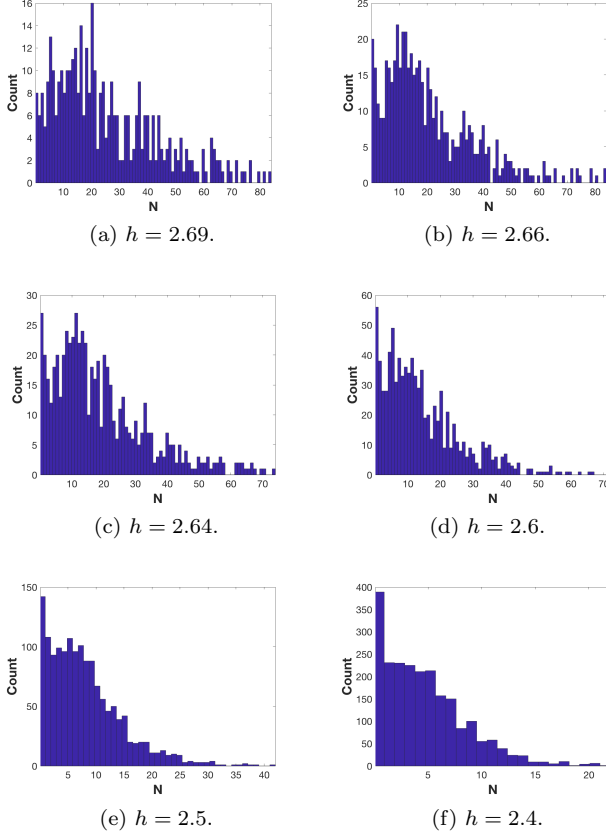


FIG. 3: Histograms of the distribution of the number of SAOs between two spikes corresponding to system (18) close to Hopf bifurcation for parameter values given by (6) and noise intensities $\sigma_1 = 10^{-6}$, $\sigma_2 = \sigma_3 = 3 \cdot 10^{-3}$.

in Fig. 3 and Fig. 4; in our numerical study, we considered oscillations in the x -variable. Oscillations whose amplitudes exceeded 0.1 with their maximum value below 0.6 in the x -coordinate were considered as SAOs. We observe that for parameter values above and close to the singular Hopf bifurcation, the distributions are multimodal with wider range, while below and away from the Hopf value, the distributions are reverse J-shaped with shorter range. Similarly, lower noise levels lead to unimodal distributions with long tails, while higher noise yield distributions that are reverse J-shaped (see Fig. 4). We conjecture that the reverse J-shaped distributions asymptotically approach an exponential distribution with increasing noise levels or distance from the Hopf bifurcation. Similar results have been shown in a planar model with multiplicative noise in³⁷. In fact, the noise-induced SAO count depends on the number of oscillations a sample path makes around the deterministically-stable small limit cycle. A large excursion occurs only if the sample path gets kicked by noise from a neighborhood of this limit cycle as shown in Fig. 5. We refer to^{9,32} for the simpler case of additive noise in planar systems, which is already highly non-trivial mathematically. We also re-

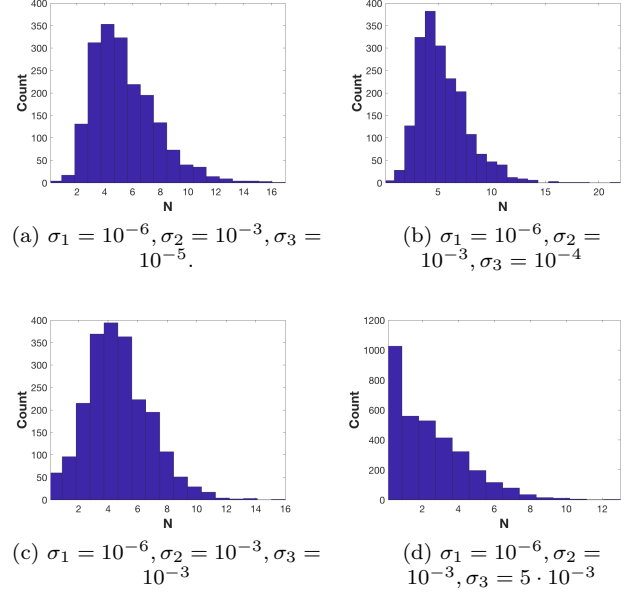


FIG. 4: Histograms of SAOs corresponding to system (18) at $h = 2.3$ for different noise intensities and parameter values given by (6).

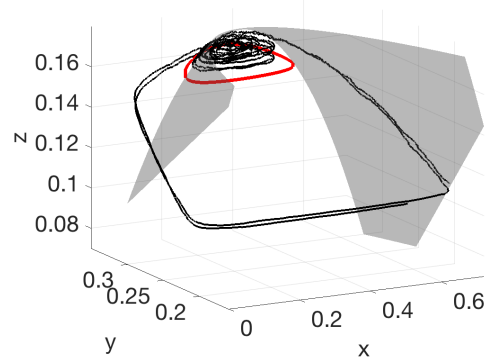


FIG. 5: A sample path of system (18) along with the deterministic stable limit cycle (plotted in red) against the critical manifold \mathcal{S} . The other parameter values are as in Fig. 4 with $\sigma_1 = 10^{-6}$, $\sigma_2 = \sigma_3 = 5 \cdot 10^{-3}$.

mark that the histograms in Fig. 3 are naturally related to ecological applications, such as the distribution of return times of outbreaks of larch budmoth in European Alps¹⁶. To make this connection more precise would be an interesting direction for future work.

Next, we numerically study the effect of noise on the return map which was discussed in Section II. We fix h at 2.3 and the other parameter values as in (6). We then consider a line segment \mathcal{L} on a plane Σ far from \mathcal{F}^+ , integrate a sample path starting on equally spaced points on \mathcal{L} forward, and record its first intersection with Σ . Fig. 6 shows the image of \mathcal{L} , where we choose Σ to be $x = 0.18$ and \mathcal{L} to be a line segment on Σ with its

y -coordinate fixed at 0.22, and z varying between 0.05 and 0.18. We observe that different deterministically discernible regions (cf. Fig. 6(b) and (f)), tend to look similar if more noise is added, i.e., the plateau disappears. Furthermore, the return maps look very regular, in certain parts even almost linear, which relates to similar observations made in²⁶ for a simpler model.

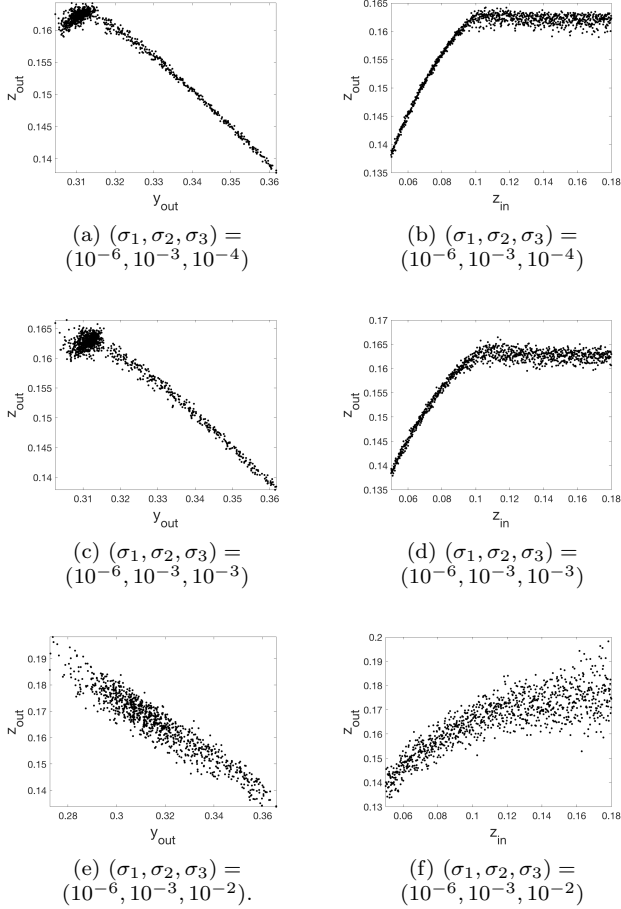


FIG. 6: Left column: Image of intersections of a grid of 1000 trajectories with Σ . Right column: Final values of z plotted against their initial values.

IV. ANALYSIS NEAR THE FOLDED SINGULARITY

The remaining step is to link our results to theoretical background, which describes whether the SAOs are purely due to noise or have been induced by deterministic mechanisms, e.g., by a folded node. Key theoretical steps to understand this effect were made in⁷. In⁷, the authors study a slow-fast stochastic system in its normal form, where they quantify the effect of additive noise and obtain critical noise intensities beyond which the SAOs become hidden by fluctuations. Hence, we may ask whether we can transform our system near a folded node into a

suitable normal form SDE.

We will focus our analysis near a folded singularity of the desingularized system (4) and follow ideas in⁴⁰, now extended to the stochastic context. Let $p^* = (x^*, y^*, z^*) \in \mathcal{F}^+$ be a fold point where the transversality condition fails, i.e. (x^*, y^*, z^*) satisfy the following:

$$\begin{cases} 1 - x^* - \frac{y^*}{\beta_1 + x^*} - \frac{z^*}{\beta_2 + x^*} &= 0 \\ -1 + \frac{y^*}{(\beta_1 + x^*)^2} + \frac{z^*}{(\beta_2 + x^*)^2} &= 0 \\ \frac{y^*}{\beta_1 + x^*} \left(\frac{x^*}{\beta_1 + x^*} - c \right) + \frac{z^*}{\beta_2 + x^*} \left(\frac{x^*}{\beta_2 + x^*} - d - h z^* \right) &= 0, \end{cases}$$

with $x^* > c\beta_1/(1-c)$, $y^*, z^* > 0$. The fold curve \mathcal{F}^+ in its parametric form is given by

$$\mathcal{F}^+ = \{(s, \phi(s), \psi(s)) : a \leq s \leq b\}, \text{ where}$$

$$\phi(s) = \frac{(\beta_1 + s)^2}{\beta_1 - \beta_2} (1 - \beta_2 - 2s),$$

$$\psi(s) = \frac{(\beta_2 + s)^2}{\beta_1 - \beta_2} (2s + \beta_1 - 1),$$

$$a = \frac{1 - \max\{\beta_1, \beta_2\}}{2}, \quad b = \frac{1 - \min\{\beta_1, \beta_2\}}{2}.$$

Let $s^* \in (a, b)$ be such that $s^* = x^*$, $\phi(s^*) = y^*$ and $\psi(s^*) = z^*$, i.e. s^* gets mapped to p^* . Then for z near z^* , we can show that \mathcal{F}^+ can be linearly approximated by $\{(c_{11}z, c_{22}z, z)\}$, where

$$c_{11} = \frac{\beta_1 - \beta_2}{2(\beta_2 + x^*)(3x^* + \beta_1 + \beta_2 - 1)}, \quad c_{22} = -\frac{\beta_1 + x^*}{\beta_2 + x^*},$$

provided that $\beta_1 \neq \beta_2$. Note that near p^* , it is easy to see that F_i can be approximated by the functions G_i with $F_i^2(x, y, z) = G_i^2(x, y, z) + O((x-x^*)^2, (y-y^*)^2, (z-z^*)^2)$ for $i = 1, 2, 3$, where

$$G_1(X, Y, Z) = \sqrt{X + X^2 + \frac{XY}{\beta_1 + X} + \frac{XZ}{\beta_2 + X}},$$

$$G_2(X, Y, Z) = \sqrt{\frac{XY}{\beta_1 + X} + c},$$

$$G_3(X, Y, Z) = \sqrt{\frac{XZ}{\beta_2 + X} + dZ + hZ^2}.$$

For the ease of calculations, we will consider system (19) with F_i replaced by G_i . Throughout our work for each positive integer k , $O(k)$ represents multivariate terms of the form $X^\alpha Y^\beta Z^\gamma$ such that $\alpha + \beta + \gamma = k$, where α, β, γ are non-negative integers.

Proposition IV.1 *Near the folded node singularity (x^*, y^*, z^*) there exists a smooth change of coordinates such that system (19) can be written in its normal form:*

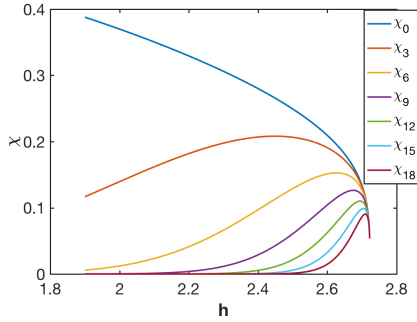
$$\begin{cases} dX_t = F_1(X_t, Y_t, Z_t)dt + \kappa\sigma_1 G_1(X_t, Y_t, Z_t) dW_t^{(1)} \\ \quad + \sqrt{\zeta}\kappa\sigma_3 c_{11} G_3(X_t, Y_t, Z_t) dW_t^{(3)} \\ dY_t = \zeta F_2(X_t, Y_t, Z_t)dt + \frac{\kappa x^* \sqrt{\zeta}}{\beta_1 + x^*} \left[(-\sigma_2 G_2(X_t, Y_t, Z_t) \right. \\ \quad \left. + O(1))dW_t^{(2)} + (\sigma_3 c_{22} G_3(X_t, Y_t, Z_t) \right. \\ \quad \left. + O(1))dW_t^{(3)} \right] \\ dZ_t = \zeta F_3(X_t, Y_t, Z_t)dt + \sqrt{\zeta}\sigma_3 G_3(X_t, Y_t, Z_t) dW_t^{(3)}, \end{cases}$$

where the functions are given by

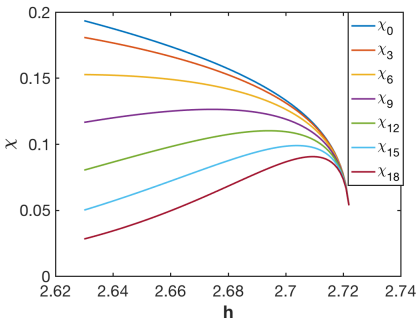
$$\begin{pmatrix} F_1 \\ F_2 \\ F_3 \end{pmatrix} = \begin{pmatrix} Y_t + X_t^2 + CX_tY_t + \zeta O(X_t, Y_t, Z_t, \zeta) + O(3) \\ A_1X_t + A_2Y_t + A_3Z_t + A_4G_3^2(X_t, Y_t, Z_t) + O(2) \\ B_0 + B_1X_t + B_2Z_t + O(2) \end{pmatrix},$$

$$\begin{pmatrix} G_1^2 \\ G_2^2 \\ G_3^2 \end{pmatrix} = \begin{pmatrix} 2x^* + \frac{2}{\kappa}X_t - Y_t + 2c_{11}Z_t - \zeta C_0 + O(2) \\ D_0 + D_1X_t + D_2Y_t + D_3Z_t - D_4\zeta + O(2) \\ E_0 + \frac{\beta_2 z^*}{\kappa(\beta_2 + x^*)}X_t + \left(\frac{\beta_2 c_{11} z^*}{(\beta_2 + x^*)^2} + h z^* \right) Z_t + O(2) \end{pmatrix},$$

with G_1 , G_2 and G_3 being the positive square roots of G_1^2 , G_2^2 and G_3^2 . The constants are all explicitly computable and given in (21)-(39).



(a) χ_k vs h



(b) A zoomed view

FIG. 7: Plots of χ_k as functions of h for different values of k and parameter values given by (6).

The proof is given in the Appendix. With this normal form, we have a very explicit tool to understand the parameter influence on the noise terms near the folded node. For instance, we consider the parameter

$$c_{11} = \frac{\beta_1 - \beta_2}{2(\beta_2 + x^*)(3x^* + \beta_1 + \beta_2 - 1)}.$$

If the two predators are similar with respect to their semi-saturation constants, i.e., $\beta_1 \approx \beta_2$, then fluctuations for the Y -predator near the folded node depend to leading-order only very weakly on the demographic noise of the

Z -predator; similar ecological parameter studies can now be carried out for various parameters and SAO counts, but we leave this aspect for future work.

In⁷, the noise level influence was carried out relative to the various canard orbits. Consider the k -th secondary canard. For each $k \in \mathbb{N}$, let

$$\chi_k(\mu) = \mu^{1/4} e^{-(2k+1)^2 \mu} \quad (20)$$

where μ is the eigenvalue ratio at the folded node defined in (5) and χ_k is the noise level for additive noise near a folded node in the normal form defined⁷. The curves $\chi_k(\mu)$ define the boundary regions in (μ, χ) -parameter space^{7,8}. To link this normal form result to our context, we plot $\mu = \mu(h)$ as a function of the main bifurcation parameter h as shown in Fig. 7. Basically, upon decreasing the noise level, within each region, we can distinguish more and more deterministic SAOs from pure-noise SAOs near a folded node.

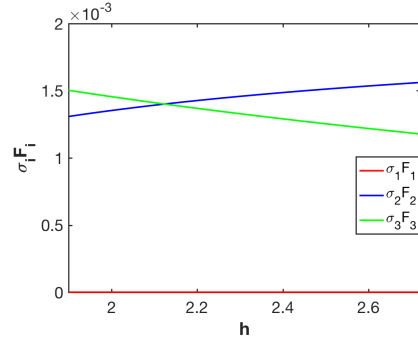


FIG. 8: The noise pre-factors $\sigma_i F_i$ corresponding to system (18) evaluated at (x^*, y^*, z^*) .

To actually link the results completely, we have to determine the noise level χ , which can be done by evaluating the products $\sigma_i F_i$ from (18) at the folded node. The results are shown in Fig. 8 for parameter values given by (6). Our noise is rather small relative to χ , so we may only expect occasional stochastic deviations from SAOs in the regime far from the singular Hopf bifurcation. However, the time series in Fig. 2 show more irregular behavior, which the theory does not cover as the SAOs occur near a singular Hopf bifurcation. The discrepancy is particularly apparent in the case when a small deterministically stable limit cycle exists; see Fig. 5. Hence, we conclude that a singular Hopf bifurcation can still produce quite irregular MMOs, even for relatively small noise levels, where a folded node normal form theory would not give an indication for the influence of noise on MMOs. To investigate this effect mathematically remains a formidable challenge for future work.

V. APPENDIX

We perform the following series of transformations to arrive at the normal form. We are going to need the

following constants to simplify the notation:

$$A_1 = -x^* \left(\frac{\beta_1 y^*}{(\beta_1 + x^*)^3} + \frac{\beta_2 z^*}{(\beta_2 + x^*)^3} \right), \quad (21)$$

$$A_2 = \frac{\beta_1 C_0}{x^*(\beta_1 + x^*)} + C_1, \quad (22)$$

$$C_0 = c_{11} z^* \left(\frac{x^*}{\beta_1 + x^*} - d - h z^* \right), \quad (23)$$

$$C_1 = \frac{x^*}{\beta_1 + x^*} - c, \quad (24)$$

$$A_3 = x^* \kappa \left[\frac{1}{\beta_2 + x^*} \left(d + 2h z^* - c - \frac{(\beta_1 - \beta_2)x^*}{(\beta_1 + x^*)(\beta_2 + x^*)} \right) - c_{11} \left(\frac{\beta_1 y^*}{(\beta_1 + x^*)^3} + \frac{\beta_2 z^*}{(\beta_2 + x^*)^3} \right) \right], \quad (25)$$

$$A_4 = \frac{c_{11} c_{22} \kappa \beta_1 \sigma_3^2 \zeta}{(\beta_1 + x^*)^2}, \quad (26)$$

$$B_0 = z^* \left(\frac{x^*}{\beta_2 + x^*} - d - h z^* \right), \quad (27)$$

$$B_1 = \frac{\beta_2 z^*}{(\beta_2 + x^*)^2}, \quad (28)$$

$$B_2 = \frac{x^*}{\beta_2 + x^*} - d - 2h z^* + \frac{c_{11} \beta_2 z^*}{(\beta_2 + x^*)^2}, \quad (29)$$

$$C = \frac{\beta_1}{\kappa x^*(\beta_1 + x^*)}, \quad (30)$$

$$D_0 = y^* \left(\frac{x^*}{\beta_1 + x^*} + c \right), \quad (31)$$

$$D_1 = \frac{\beta_1 y^*}{\kappa(\beta_1 + x^*)^2}, \quad (32)$$

$$D_2 = -\frac{c\beta_1 + (1+c)x^*}{x^*}, \quad (33)$$

$$D_3 = \frac{c_{11} \beta_1 y^*}{(\beta_1 + x^*)^2}, \quad (34)$$

$$D_4 = \frac{c_{11} B_0}{x^*} (c\beta_1 + (1+c)x^*), \quad (35)$$

$$E_0 = z^* \left(\frac{x^*}{\beta_2 + x^*} + d + h z^* \right), \quad (36)$$

$$\kappa = -x^* \left(\frac{y^*}{(\beta_1 + x^*)^3} + \frac{z^*}{(\beta_2 + x^*)^3} \right), \quad (37)$$

$$c_{11} = \frac{\beta_1 - \beta_2}{2(\beta_2 + x^*)(3x^* + \beta_1 + \beta_2 - 1)}, \quad (38)$$

$$c_{22} = -\frac{\beta_1 + x^*}{\beta_2 + x^*}. \quad (39)$$

The main procedure consists of four main steps.

1) Translation to the origin: $X \mapsto X + x^*$, $Y \mapsto Y + y^*$, $Z \mapsto Z + z^*$. The transformed system reads as

$$\begin{cases} dX = f_1(X, Y, Z) dt + \sigma_1 G_1(X, Y, Z) dW_t^{(1)} \\ dY = \zeta f_2(X, Y, Z) dt + \sigma_2 \sqrt{\zeta} G_2(X, Y, Z) dW_t^{(2)} \\ dZ = \zeta f_3(X, Y, Z) dt + \sigma_3 \sqrt{\zeta} G_3(X, Y, Z) dW_t^{(3)}, \end{cases}$$

where the drift are specified further by the functions

$$\begin{pmatrix} f_1 \\ f_2 \\ f_3 \end{pmatrix} = \begin{pmatrix} (X + x^*) \left(1 - (X + x^*) - \frac{Y + y^*}{\beta_1 + X + x^*} - \frac{Z + z^*}{\beta_2 + X + x^*} \right) \\ (Y + y^*) \left(\frac{X + x^*}{\beta_1 + X + x^*} - c \right) \\ (Z + z^*) \left(\frac{X + x^*}{\beta_2 + X + x^*} - d - h(Z + z^*) \right) \end{pmatrix},$$

and the diffusion terms are fully defined via the functions

$$\begin{pmatrix} G_1 \\ G_2 \\ G_3 \end{pmatrix} = \begin{pmatrix} \sqrt{X + x^*} \sqrt{1 + (X + x^*) + \frac{Y + y^*}{\beta_1 + X + x^*} + \frac{Z + z^*}{\beta_2 + X + x^*}} \\ \sqrt{Y + y^*} \sqrt{\frac{X + x^*}{\beta_1 + X + x^*} + c} \\ \sqrt{Z + z^*} \sqrt{\frac{X + x^*}{\beta_2 + X + x^*} + d + h(Z + z^*)} \end{pmatrix}.$$

2) Rectification of the fold curve to the z -axis: $X = \tilde{X} + c_{11} \tilde{Z}$, $Y = \tilde{Y} + c_{22} \tilde{Z}$, $Z = \tilde{Z}$, where c_{11} and c_{22} are defined by (38)-(39). The transformed system reads as

$$\begin{cases} d\tilde{X} = \tilde{f}_1(\tilde{X}, \tilde{Y}, \tilde{Z}) dt + \sigma_1 \tilde{G}_1(\tilde{X}, \tilde{Y}, \tilde{Z}) dW_t^{(1)} \\ \quad - \sqrt{\zeta} c_{11} \sigma_3 \tilde{G}_3(\tilde{X}, \tilde{Y}, \tilde{Z}) dW_t^{(3)} \\ d\tilde{Y} = \zeta \tilde{f}_2(\tilde{X}, \tilde{Y}, \tilde{Z}) dt + \sqrt{\zeta} (\sigma_2 \tilde{G}_2(\tilde{X}, \tilde{Y}, \tilde{Z}) dW_t^{(2)} \\ \quad - c_{22} \sigma_3 \tilde{G}_3(\tilde{X}, \tilde{Y}, \tilde{Z}) dW_t^{(3)}) \\ d\tilde{Z} = \zeta \tilde{f}_3(\tilde{X}, \tilde{Y}, \tilde{Z}) dt + \sigma_3 \sqrt{\zeta} \tilde{G}_3(\tilde{X}, \tilde{Y}, \tilde{Z}) dW_t^{(3)}, \end{cases}$$

where

$$\begin{pmatrix} \tilde{f}_1 \\ \tilde{f}_2 \\ \tilde{f}_3 \end{pmatrix} = \begin{pmatrix} -\frac{x^*}{\beta_1 + x^*} \tilde{Y} - \frac{D_3}{y^*} \tilde{Y} \tilde{Z} + \kappa \tilde{X}^2 - \frac{D_3}{c_{11} y^*} \tilde{X} \tilde{Y} \\ -\zeta c_{11} L + O(3) \\ -\frac{A_1}{x^*} (\beta_1 + x^*) \tilde{X} + \left(\frac{x^*}{(\beta_1 + x^*)^3} - c \right) \tilde{Y} + M \tilde{Z} \\ + O(2) \\ B_0 + B_1 \tilde{X} + B_2 \tilde{Z} + O(2) \end{pmatrix},$$

and we also have

$$L(\tilde{X}, \tilde{Y}, \tilde{Z}) = B_0 + B_1 \tilde{X} + B_2 \tilde{Z} + O(2),$$

$$M = -\frac{A_3(\beta_1 + x^*)}{x^* \kappa},$$

with A_1 defined by (21), A_3 by (25), B_i for $i = 0, 1, 2$ by (27)-(29), D_3 by (34) and κ by (37). The functions \tilde{G}_i for $i = 1, 2, 3$ are positive square roots of \tilde{G}_i^2 , where

$$\begin{pmatrix} \tilde{G}_1^2 \\ \tilde{G}_2^2 \\ \tilde{G}_3^2 \end{pmatrix} = \begin{pmatrix} 2x^* + 2\tilde{X} + \frac{x^*}{\beta_1 + x^*} \tilde{Y} + 2c_{11} \tilde{Z} + O(2) \\ D_0 + \frac{\beta_1 y^*}{(\beta_1 + x^*)^2} \tilde{X} + \left(\frac{x^*}{\beta_1 + x^*} + c \right) \tilde{Y} + D_3 \tilde{Z} \\ + O(2) \\ E_0 + B_1 \tilde{X} + z^* \left(\frac{\beta_2 c_{11}}{(\beta_2 + x^*)^2} + h \right) \tilde{Z} + O(2) \end{pmatrix}$$

with D_0 and E_0 defined by (31) and (36) respectively.

3) Stretch and translation of the coordinates \tilde{X} and \tilde{Y} :

$$\hat{X} = \kappa \tilde{X}, \hat{Y} = -\frac{x^* \kappa}{\beta_1 + x^*} \tilde{Y} - \zeta c_{11} \kappa E_0, \hat{Z} = \tilde{Z}.$$

The transformed system reads as

$$\begin{cases} d\hat{X} = \hat{f}_1(\hat{X}, \hat{Y}, \hat{Z}) dt + \kappa \left[\sigma_1 \hat{G}_1(\hat{X}, \hat{Y}, \hat{Z}) dW_t^{(1)} - \sqrt{\zeta} c_{11} \sigma_3 \hat{G}_3(\hat{X}, \hat{Y}, \hat{Z}) dW_t^{(3)} \right] \\ d\hat{Y} = \zeta \hat{f}_2(\hat{X}, \hat{Y}, \hat{Z}) dt - \frac{x^* \kappa \sqrt{\zeta}}{\beta_1 + x^*} \left[\sigma_2 \hat{G}_2(\hat{X}, \hat{Y}, \hat{Z}) dW_t^{(2)} - c_{22} \sigma_3 \hat{G}_3(\hat{X}, \hat{Y}, \hat{Z}) dW_t^{(3)} \right] \\ d\hat{Z} = \zeta \hat{f}_3(\hat{X}, \hat{Y}, \hat{Z}) dt + \sigma_3 \sqrt{\zeta} \hat{G}_3(\hat{X}, \hat{Y}, \hat{Z}) dW_t^{(3)}, \end{cases}$$

where

$$\begin{pmatrix} \hat{f}_1 \\ \hat{f}_2 \\ \hat{f}_3 \end{pmatrix} = \begin{pmatrix} (1 + c_{11} \kappa C \hat{Z}) \hat{Y} + \hat{X}^2 + \kappa C \hat{X} \hat{Y} + O(\zeta) + O(3) \\ A_1 \hat{X} + C_1 \hat{Y} + A_3 \hat{Z} + \zeta c_{11} \kappa B_0 C_1 + O(2) \\ B_0 + B_1 \hat{X} + B_2 \hat{Z} + O(2) \end{pmatrix}$$

and

$$\begin{pmatrix} \hat{G}_1 \\ \hat{G}_2 \\ \hat{G}_3 \end{pmatrix} = \begin{pmatrix} 2x^* + \frac{2}{\kappa} \hat{X} - \frac{1}{\kappa} \hat{Y} - \zeta c_{11} B_0 + 2c_{11} \hat{Z} + O(2) \\ D_0 + D_1 \hat{X} + D_2 \hat{Y} + D_3 \hat{Z} + \zeta c_{11} B_0 D_2 + O(2) \\ B_0 + \frac{B_1}{\kappa} \hat{X} + \left(\frac{\beta_2 c_{11} z^*}{(\beta_2 + x^*)^2} + h z^* \right) \hat{Z} + O(2) \end{pmatrix}$$

with C defined by (30), D_i by (31)-(34) and \hat{G}_i being the positive square root of \hat{G}_i^2 for $i = 0, 1, 2, 3$.

4) A final transformation of \hat{X} and \hat{Y} : $\bar{X} = \hat{X}$, $\bar{Y} = \left(1 + \frac{c_{11} \beta_1}{x^* (\beta_1 + x^*)}\right) \hat{Y}$, $\bar{Z} = \hat{Z}$. Carrying out this transformation, dropping the overbars, and denoting the components by (X_t, Y_t, Z_t) , we thus obtain the proposition.

- ¹E. Allen, *Modeling with Itô Stochastic Differential Equations*, Springer 2007.
- ²L. Allen, *An Introduction to Stochastic Processes With Applications to Biology*, Chapman and Hall/CRC 2010.
- ³C. Asaro and L.A. Chamberlin, *Outbreak History (1953 – 2014) of Spring Defoliators Impacting Oak-Dominated Forests in Virginia, with Emphasis on Gypsy Moth (Lymantria dispar L.) and Fall Cankerworm (Alsophila pomataria Harris)*, American Entomologist (2015) 174-185.
- ⁴E. Benoît. Canards et enlacements. *Publ. Math. IHES*, 72:63–91, 1990.
- ⁵R. Benzi, A. Sutera, and A. Vulpiani. The mechanism of stochastic resonance. *J. Phys. A*, 14(11):453–457, 1981.
- ⁶N. Berglund and B. Gentz. *Noise-Induced Phenomena in Slow-Fast Dynamical Systems*. Springer, 2006.
- ⁷N. Berglund, B. Gentz and C. Kuehn, *Hunting French ducks in a noisy environment*, *J. Diff. Eqns* 252 (2012) 4786-4841.
- ⁸N. Berglund, B. Gentz, and C. Kuehn. From random Poincaré maps to stochastic mixed-mode-oscillation patterns. *J. Dyn. Diff. Equat.*, 27(1):83–136, 2015.
- ⁹N. Berglund and D. Landon. Mixed-mode oscillations and interspike interval statistics in the stochastic FitzHugh-Nagumo model. *Nonlinearity*, 25:2303–2335, 2012.
- ¹⁰B. Braaksma. Singular Hopf bifurcation in systems with fast and slow variables. *J. Nonlinear Sci.*, 8(5):457–490, 1998.
- ¹¹B.M. Brøns, M. Krupa, M. Wechselberger, *Mixed Mode Oscillations Due to the Generalized Canard Phenomenon*, Fields Institute Communications 49 (2006) 39-63.
- ¹²F. Campillo and C. Lobry, *Effect of population size in a predator-prey model*, *Eco. Modelling* 246 (2012) 1-10.
- ¹³P. Chesson, *Predator-Prey Theory and Variability*, Annual Rev. Eco. Systematics 9 (1978) 323-347.

- ¹⁴B. Deng, *Food chain chaos due to junction-fold point*, *Chaos* 11 (2001) 514-525.
- ¹⁵M. Desroches, J. Guckenheimer, B. Krauskopf, C. Kuehn, H.M. Osinga, M. Wechselberger, *Mixed-Mode Oscillations with Multiple time-scales*, *SIAM Review* 54 (2012) 211-288.
- ¹⁶J. Esper, U. Buñitgen, D.C. Frank, D. Nievergelt, and A. Liebhold, *1200 years of regular outbreaks in alpine insects*, *Proc. R. Soc. B* (2007) 274, 671-679.
- ¹⁷N. Fenichel. Geometric singular perturbation theory for ordinary differential equations. *J. Differential Equat.*, 31:53–98, 1979.
- ¹⁸L. Gammaitoni, P. Hänggi, P. Jung, and F. Marchesoni. Stochastic resonance. *Rev. Mod. Phys.*, 70:223–287, 1998.
- ¹⁹C. Gardiner. *Stochastic Methods*. Springer, Berlin Heidelberg, Germany, 4th edition, 2009.
- ²⁰J. Guckenheimer. Singular Hopf bifurcation in systems with two slow variables. *SIAM J. Appl. Dyn. Syst.*, 7(4):1355–1377, 2008.
- ²¹G. Hek, *Geometric singular perturbation theory in biological practice*, *J. Math. Biol.* 60 (2010) 347-386.
- ²²D.J. Higham. An algorithmic introduction to numerical simulation of stochastic differential equations. *SIAM Review*, 43(3):525–546, 2001.
- ²³E. Korpimäki, P.R. Brown, J. Jacob, and R.P. Pech, *The Puzzles of Population Cycles and Outbreaks of Small Mammals Solved?*, *BioScience* 54 (2004), 1071-1079.
- ²⁴M. Krupa and P. Szmolyan. Extending slow manifolds near transcritical and pitchfork singularities. *Nonlinearity*, 14:1473–1491, 2001.
- ²⁵M. Krupa and M. Wechselberger. Local analysis near a folded saddle-node singularity. *J. Differential Equat.*, 248(12):2841–2888, 2010.
- ²⁶C. Kuehn, *On decomposing mixed-mode oscillations and their return maps*, *Chaos* 21 (2011) 1-15.
- ²⁷C. Kuehn. Time-scale and noise optimality in self-organized critical adaptive networks. *Phys. Rev. E*, 85(2):026103, 2012.
- ²⁸C. Kuehn, *Multiple Time Scale Dynamics*, Springer, 2015. 814 pp.
- ²⁹C. Kuehn and P. Szmolyan. Multiscale geometry of the Olsen model and non-classical relaxation oscillations. *J. Nonlinear Sci.*, 25(3):583–629, 2015.
- ³⁰B. Lindner and L. Schimansky-Geier. Coherence and stochastic resonance in a two-state system. *Phys. Rev. E*, 61(6):6103–6110, 2000.
- ³¹G. Meurant, *Insect Outbreaks*, Academic Press, 1987.
- ³²C.B. Muratov and E. Vanden-Eijnden. Noise-induced mixed-mode oscillations in a relaxation oscillator near the onset of a limit cycle. *Chaos*, 18:015111, 2008.
- ³³C. Nicolis and G. Nicolis. Stochastic aspects of climatic transitions—additive fluctuations. *Tellus*, 33(3):225–234, 1981.
- ³⁴S. Rinaldi and S. Muratori, *Slow-fast limit cycles in predator-prey models*, *Ecological Modelling* 61 (1992) 287-308.
- ³⁵S. Sadhu, *Mixed mode oscillations and chaotic dynamics in a two-trophic ecological model with Holling Type II functional response*, *Bull. Cal. Math. Soc.*, 106 (6) (2015) 429-442.
- ³⁶S. Sadhu, *Canards and mixed-mode oscillations in a singularly perturbed two predators-one prey model*, *Proc. Dyn. Systems and Appln.* 7 (2016) 211-219.
- ³⁷S. Sadhu, *Stochasticity Induced Mixed-mode Oscillations and Distribution of Recurrent Outbreaks in an Ecosystem*, *Chaos* (in press).
- ³⁸S. Sadhu and S. Chakraborty Thakur, *Uncertainty and Predictability in Population Dynamics of a Two-trophic Ecological Model: Mixed-mode Oscillations, Bistability and Sensitivity to Parameters*, *Ecological Complexity* (in press).
- ³⁹P. Szmolyan, M. Wechselberger, *Canards in \mathbb{R}^3* , *J. Differential Equations* 177 (2001) 419-453.
- ⁴⁰M. Wechselberger. *Singularly perturbed folds and canards in \mathbb{R}^3* . PhD thesis, Vienna University of Technology, Vienna, Austria, 1998.
- ⁴¹M. Wechselberger, *Existence and bifurcation of canards in \mathbb{R}^3 in the case of a folded node*, *SIAM J. Appl. Dyn. Syst.* 4 (1) (2005) 101-139.